Anamorphic optical transformation of an amplitude spatial light modulator to a complex spatial light modulator with square pixels [Invited]

Hwi Kim,[1] Chi-Young Hwang,[2] Kwang-Soo Kim,[3] Jinyoung Roh,[1] Woonchan Moon,[3] Sungmin Kim,[3] Beom-Ryoel Lee,[2] Seungtaik Oh,[2] and Joonku Hahn[3,*]

[1]ICT Convergence Technology for Health & Safety and Department of Electronics and Information Engineering, Korea University, 2511 Sejong-ro, Sejong 339-700, South Korea

[2]Content Research Division, Electronics and Telecommunications Research Institute, 161, Gajeong-dong, Yuseon-gu, Daejeon 305-700, South Korea

[3]School of Electronics Engineering, Kyungpook National University, 1370 Sankyuk-dong, Buk-gu, Daegu 702-701, South Korea

*Corresponding author: jhahn@knu.ac.kr

Received 4 June 2014; revised 7 July 2014; accepted 8 July 2014; posted 9 July 2014 (Doc. ID 213478); published 11 August 2014

A method is proposed for the construction of a square pixel complex spatial light modulator (SLM) from a commercial oblong full-high-definition (full-HD) amplitude SLM using an anamorphic optical filter. In the proposed scheme, one half-band of the optical Fourier transform of the amplitude-only spatial light field is rejected in the optical Fourier plane and the other half-band is reformatted to be an effective complex SLM with square pixels. This has an advantage in the viewing window plane since the shape of the viewing window becomes square and more ideal for observers who watch the hologram contents through it. For optimal transformation, the amplitude computer generated hologram encoding scheme was developed. Mathematical modeling of the proposed system is described herein, and it was experimentally demonstrated that the effective complex SLM displays complex holographic three-dimensional images with a clear depth discrimination effect.

OCIS codes: (090.1995) Digital holography; (090.2870) Holographic display; (070.6110) Spatial filtering.

http://dx.doi.org/10.1364/AO.53.00G139

1. Introduction

An optical wave field is generally characterized by two independent variables at a given point, i.e., the phase and amplitude. Theoretically, complex spatial light modulators (SLMs) can generate perfect optical wave fields with controlled amplitudes and phases. However, in practice, such a complex SLM has not yet been reported and most available SLMs are designed to be in the form of amplitude-only or phase-only SLMs with only one degree of freedom.

Complex SLMs may be essential for the development of various wave optic applications such as holographic tomography, microscopy, turbid medium power transfer, and holographic display. Complex SLMs are particularly crucial for advancing holographic three-dimensional (3D) display technology [1]. Unlike other 3D display technologies, holographic 3D display technology creates the complete wave field containing both phase and amplitude information. Consequently, the holographic 3D display is considered to be the ultimate form of 3D display. It is expected that holographic 3D display using complex SLMs will be able to provide the most natural 3D images with features such as a continuous

1559-128X/14/27G139-08$15.00/0

parallax, the accommodation effect, and, in particular, a low optical noise level.

Holographic 3D displays and associated hologram encoding schemes have been actively researched [2–8]. In practice, it is difficult to modulate complex optical fields; therefore, indirect complex field encoding methods have been actively investigated to make so called macro-pixel structures. There has been research on binary amplitude encoding [9], detour phase encoding [10,11], double phase hologram (DPH) encoding [12,13], and single-sideband holography [14]. When a complex hologram is encoded on an SLM according to the single-sideband holography method, the bandwidth of the hologram needs to be limited to within half of the Nyquist frequency in order to separate the signal from its conjugate. Similar off-axis hologram encoding concepts have been studied. However, as will be elucidated further in this paper, the nonsquare pixels produced by macro-pixel schemes cause different horizontal and vertical resolutions.

In this paper, we consider the practical problem of synthesizing an effective complex SLM with square pixels using conventional full-high-definition (full-HD) amplitude-type SLMs. Composite complex fields were generated through the amplitude-type computer generated hologram (CGH) encoding method by the formation of macro-pixels from two adjacent amplitude pixels. The fields were then analyzed in terms of wave optics. The process requires a thorough understanding of the principles behind the formation of effective complex modulation pixels. An anamorphic optical transformation system with a Fourier optical filter is proposed, which transforms an amplitude SLM into an effective complex SLM with square pixels, i.e., pixels of equal horizontal and vertical dimensions. Such square pixel complex SLMs are useful in practice for generating full-parallax holographic images featuring the same viewing angles along the x axial and y axial directions. This is meaningful since this ratio determines the shape of the viewing window through which the observer watches holographic 3D images. The proposed system was verified through experimental reconstruction of holographic 3D images and demonstrates both the depth-discrimination effect, i.e., accommodation effect, and anamorphic optical transformation.

2. Complex Encoding on the Amplitude-Only Spatial Light Modulator

Optical waves have complex information with real and imaginary terms, or alternatively amplitude and phase. Therefore, in order to reconstruct complex optical waves perfectly, two independent variables are required for each given point. The theoretically simplest solution is to build a complex modulator with two control parameters for each pixel. However, in practice, most SLMs are designed for commercial display devices such as LCD and liquid crystal on silicon (LCoS) displays. The

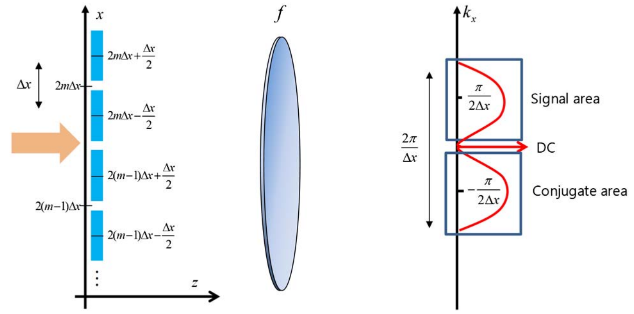

Fig. 1. Optical Fourier transform of amplitude modulation pixels and its field distribution at the Fourier domain.

manufacture of such a specialized complex modulation device from scratch may be unfeasible.

Therefore, we take a different approach using a macro-pixel structure that groups two adjacent pixels. Figure 1 shows the optical conversion process of two adjacent amplitude pixels at $x = 2m\Delta x + \Delta x/2$ and $x = 2m\Delta x - \Delta x/2$, which are encoded by the values of $A_m[\cos(k_c(2m + 1/2)\Delta x + \phi_m) + 1]$ and $A_m[\cos(k_c(2m - 1/2)\Delta x + \phi_m) + 1]$, respectively. The lower macro-pixel at $x = 2(m - 1)\Delta x$ shown in Fig. 1 is encoded by $A_{m-1}[\cos(k_c(2(m - 1) \pm 1/2)\Delta x + \phi_{m-1}) + 1]$. Here, Δx and m are the pixel pitch and pixel index, respectively. A_m and ϕ_m are the amplitude and phase, respectively, and k_c is the carrier frequency of the amplitude encoding.

This encoding scheme is applied to the amplitude SLM panel and then the total optical transmittance function of the amplitude SLM can be represented as

$$\begin{aligned} T(x) = \sum_{m=-M}^{M} \Bigg[& A_m\left[\cos\left(k_c\left(2m+\frac{1}{2}\right)\Delta x+\phi_m\right)+1\right] \\ & \times \mathrm{rect}\left(\frac{x-\left(2m+\frac{1}{2}\right)\Delta x}{\Delta x}\right) \\ & + A_m\left[\cos\left(k_c\left(2m-\frac{1}{2}\right)\Delta x+\phi_m\right)+1\right] \\ & \times \mathrm{rect}\left(\frac{x-\left(2m-\frac{1}{2}\right)\Delta x}{\Delta x}\right)\Bigg]. \end{aligned} \tag{1a}$$

The optical field with modulated amplitude is transferred by a singlet of focal length f, then the optical Fourier transform is obtained at the focal plane of the singlet as shown in Fig. 1. The transmittance function Eq. (1a) is written in the form of the sum of the real number amplitude modulation and the zeroth-order diffracted light (DC) term as

$$T(x)=\sum_{m=-M}^{M}\left[A_m\cos\left(k_c\left(2m+\frac{1}{2}\right)\Delta x+\phi_m\right)\right.$$
$$\times\mathrm{rect}\left(\frac{x-\left(2m+\frac{1}{2}\right)\Delta x}{\Delta x}\right)$$
$$+A_m\cos\left(k_c\left(2m-\frac{1}{2}\right)\Delta x+\phi_m\right)$$
$$\left.\times\mathrm{rect}\left(\frac{x-\left(2m-\frac{1}{2}\right)\Delta x}{\Delta x}\right)\right]$$
$$+\mathrm{rect}\left(\frac{x}{(2M+1)\Delta x}\right). \tag{1b}$$

The transmittance function, $T(x)$, has an angular spectrum, $F(k_x)$, obtained by [15]

$$F(k_x)=\int_{-\infty}^{\infty}T(x)\exp(-jk_x x)\mathrm{d}x$$
$$=\sum_{m=-M}^{M}\left[A_m\cos\left(k_c\left(2m+\frac{1}{2}\right)\Delta x+\phi_m\right)\right.$$
$$\times\exp\left(-jk_x\left(2m+\frac{1}{2}\right)\Delta x\right)$$
$$+A_m\cos\left(k_c\left(2m-\frac{1}{2}\right)\Delta x+\phi_m\right)$$
$$\left.\times\exp\left(-jk_x\left(2m-\frac{1}{2}\right)\Delta x\right)\right]\times\Delta x\,\mathrm{sinc}\left(\frac{k_x\Delta x}{2\pi}\right)$$
$$+(2M+1)\Delta x\,\mathrm{sinc}\left(\frac{k_x(2M+1)\Delta x}{2\pi}\right). \tag{2a}$$

The internal part of Eq. (2a) can be manipulated as follows:

$$A_m\cos\left(k_c\left(2m+\frac{1}{2}\right)\Delta x+\phi_m\right)\exp\left(-jk_x\left(2m+\frac{1}{2}\right)\Delta x\right)$$
$$+A_m\cos\left(k_c\left(2m-\frac{1}{2}\right)\Delta x+\phi_m\right)\exp\left(-jk_x\left(2m-\frac{1}{2}\right)\Delta x\right)$$
$$=A_m\exp(j\phi_m)\exp(j((k_c-k_x)(2m)\Delta x))$$
$$\times\cos\left((k_c-k_x)\frac{1}{2}\Delta x\right)+A_m\exp(-j\phi_m)$$
$$\times\exp(-j((k_c+k_x)(2m)\Delta x))\cos\left((k_c+k_x)\frac{1}{2}\Delta x\right). \tag{2b}$$

Then, by substituting Eq. (2b) into Eq. (2a), we obtain the angular spectrum $F(k_x)$:

$$F(k_x)=\Delta x\,\mathrm{sinc}\left(\frac{k_x\Delta x}{2\pi}\right)\cos\left((k_c-k_x)\frac{1}{2}\Delta x\right)$$
$$\times\sum_{m=-M}^{M}[A_m\exp(j\phi_m)\exp(j((k_c-k_x)(2m)\Delta x))]$$
$$+\Delta x\,\mathrm{sinc}\left(\frac{k_x\Delta x}{2\pi}\right)\cos\left((k_c+k_x)\frac{1}{2}\Delta x\right)$$
$$\times\sum_{m=-M}^{M}[A_m\exp(-j\phi_m)\exp(-j((k_c$$
$$+k_x)(2m)\Delta x))]$$
$$+(2M+1)\Delta x\,\mathrm{sinc}\left(\frac{k_x(2M+1)\Delta x}{2\pi}\right). \tag{2c}$$

The angular spectrum Eq. (2c) analyzes the optical information of the amplitude-only SLM through three terms: the signal term (the first term), the conjugate term (the second term), and the DC term (the third term) given, respectively, by

$$F_{\mathrm{signal}}(k_x)=\Delta x\,\mathrm{sinc}\left(\frac{k_x\Delta x}{2\pi}\right)\cos\left((k_c-k_x)\frac{1}{2}\Delta x\right)$$
$$\times\sum_{m=-M}^{M}[A_m\exp(j\phi_m)$$
$$\times\exp(j((k_c-k_x)(2m)\Delta x))], \tag{3a}$$

$$F_{\mathrm{conjugate}}(k_x)=\Delta x\,\mathrm{sinc}\left(\frac{k_x\Delta x}{2\pi}\right)\cos\left((k_c+k_x)\frac{1}{2}\Delta x\right)$$
$$\times\sum_{m=-M}^{M}[A_m\exp(-j\phi_m)$$
$$\times\exp(-j((k_c+k_x)(2m)\Delta x))], \tag{3b}$$

$$F_{\mathrm{DC}}(k_x)=(2M+1)\Delta x\,\mathrm{sinc}\left(\frac{k_x(2M+1)\Delta x}{2\pi}\right). \tag{3c}$$

Separating the signal from Eq. (2c) requires several conditions to be met. First, the separability of the noise terms from the signal is affected by the parameters k_c and M. Let us consider the effect of M. As M increases, the main lobe width of the DC term, $F_{\mathrm{DC}}(k_x)$, is squeezed into a very narrow region around $k_x=0$ and, simultaneously, the intensity of the side-lobes distributed throughout the whole region reduces. For large M, the side-lobes are negligible and most of the energy is focused around $k_x=0$. Therefore, this DC component can be easily removed by using a simple bandpass Fourier filter [15]. However, if we consider an extreme case of $M=0$, meaning that the SLM is just composed of two pixels, i.e., one macro-pixel, then the DC component broadens in the k_x space and cannot be simply separated from the signal term. Thus, the encoding scheme is conditional on having a large M. From the first and second terms, the ratio of the signal to the conjugate term is identified by

$$\text{signal:conjugate} = \cos\left((k_c - k_x)\frac{1}{2}\Delta x\right) : \cos\left((k_c + k_x)\frac{1}{2}\Delta x\right). \quad (4)$$

In the case of $(k_c + k_x)\Delta x = \pi$, the weight of the conjugate noise becomes zero. If we set $k_x = \pi/(2\Delta x)$ as the conjugate-free position, the carrier frequency k_c is obtained by $k_c = \pi/(2\Delta x)$. The weight of the conjugate term is nonzero when $k_x \neq \pi/(2\Delta x)$, meaning that the conjugate term is mixed with the signal across the whole plane.

The second condition is that, as represented by Fig. 2(b), the signal $A_m \exp(j\phi_m)$ should be band-limited to minimize contamination by the conjugate term. Regardless of the weighting ratio of Eq. (3), the signal and conjugate terms are designed to be band-limited and restricted in the single-side band. This concept has been used in off-axis holography and digital holography. The band-limited signal design is intuitively summarized for a simple one-dimensional case in Fig. 2. Figure 2(a) shows the magnitude distribution of the spatial frequency spectrum, $G_0(k_x)$. First of all, the frequency spectrum should be properly shifted with carrier frequency $k_c = \pi/(2\Delta x)$. Then, as shown in Fig. 2(b), the frequency band of the signal is selected from between 0 and $k_{x,\max}$ to avoid aliasing in the next step. Next, the real part of the wave signal in Fig. 2(b) is chosen by adding its conjugate. As can be seen from Fig. 2(c), the frequency spectrum of the real-valued signal is symmetric with respect to $f = 0$. Lastly, the appropriate DC offset is added to generate non-negative signal values as can be seen in Fig. 2(d). The resulting encoded hologram can be directly inserted into the amplitude SLM.

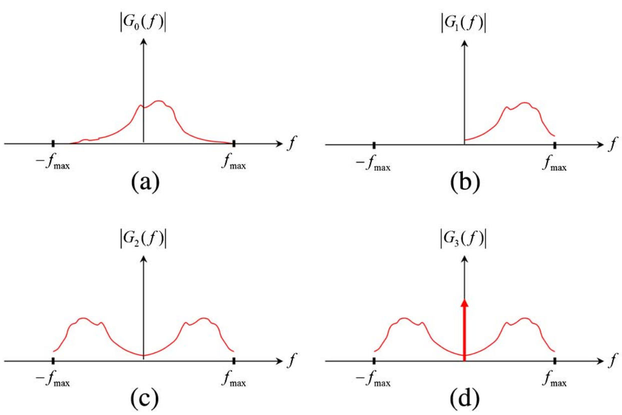

Fig. 2. Spatial frequency distributions of (a) an original target wave, (b) a shifted target wave with a carrier frequency, and (c) a target and its conjugate waves. (d) Spatial frequency distributions of the encoded non-negative real hologram.

The mentioned band-limited signal design coincides with the amplitude encoding scheme described in Eq. (1a). In the transformation process, the DC and conjugate components of the encoded hologram can be eliminated without deteriorating the signal term by filtering in the Fourier domain. Additionally, we need to address the term $\Delta x\,\mathrm{sinc}(k_x\Delta x/(2\pi))$ in Eqs. (3a) and (3b), which defines the pixel apodization. The signal is band-limited to $0 \leq k_x \leq \pi/\Delta x$. The filtering causes pixel broadening. The transmittance function of the effective complex SLM is the inverse Fourier transform of the filtered angular spectrum confined to the range $0 \leq k_x \leq \pi/\Delta x$. The resulting modulation profile is represented by

$$\begin{aligned} T_{\mathrm{cpx}}(x) &= \int_0^{\pi/\Delta x} F_{\mathrm{signal}}(k_x)\exp(jk_x x)dk_x \\ &\cong \sum_{m=-M}^{M} A_m \exp(j\phi_m)\exp(jk_c(2m\Delta x)) \\ &\quad \times \int_0^{\pi/\Delta x} \Delta x\,\mathrm{sinc}\left(\frac{k_x\Delta x}{2\pi}\right) \\ &\quad \times \exp(jk_x(x - 2m\Delta x))dk_x. \end{aligned} \quad (5)$$

The integral in Eq. (5) depicts the apodization profile of the complex modulation pixel positioned at $x = 2m\Delta x$. The pixel profile of the amplitude SLM is a rectangular function of width Δx. The optical filtering process not only broadens the pixel width but also imposes the apodization profile onto the pixel. The single-side band filtering step produces pixel apodization of width $2\Delta x$. The pixel apodization of the complex SLM is compared with that of the amplitude SLM in Fig. 3(a). Consequently, the effective complex modulation function of Eq. (5) is schematically represented in Fig. 3(b). The complex modulation pixel is simply depicted as a rectangular pixel of width $2\Delta x$ with complex modulation $A_m \exp(j\phi_m)$ as shown in Fig. 3(b). Thus far, a simple and clear explanation of the encoding method for a complex hologram has been given and its corresponding mathematical model has been described.

3. Reconstruction of Amplitude Hologram Encoding of the Full-HD CGH with an Anamorphic Fourier Filter

The basic system for converting a two-dimensional (2D) amplitude SLM to a 2D complex SLM is the $4f$ symmetric optical system shown in Fig. 4. Two pixels in the horizontal direction (x axis) are combined as a macro-pixel and the signal filtering using a half-bandpass filter occurs at the Fourier filter plane. Higher order diffraction as well as the DC and conjugate terms are filtered out to synthesize the complex SLM.

In practice, this optical transformation poses an engineering problem in that the SLM of full-HD resolution (1920 × 1080) and with square pixels has an inevitable oblong rectangular panel. In Fig. 4, the

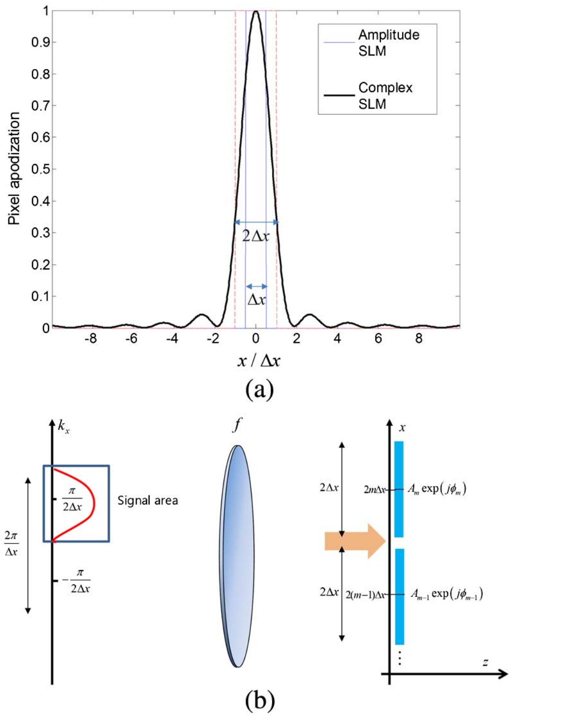

Fig. 3. (a) Pixel apodization and (b) optical filtering of the signal at the Fourier domain and its reconstruction leading to a complex modulation pixel.

resolutions and active areas of the complex and amplitude SLMs are compared. Since the $4f$ symmetric imaging system has the same magnification along the x- and y-directions, the area of the active region does not change. The Fourier filter inserted into the intermediate Fourier plane that restricts the passband to a half-plane in the x-direction increases the x-directional pixel size to $2\Delta x$. This half-band filtering creates a rectangular rather than square pixel as shown in Fig. 4.

Our main concern in this section is the optical formation of a complex SLM with a square rather than rectangular pixels. Forming square pixels with the complex SLM is important practically because it allows for the generation of full-parallax holographic

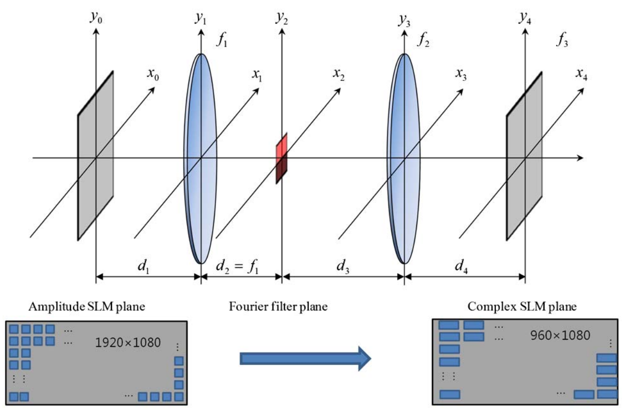

Fig. 4. Transformation of an amplitude SLM to a complex SLM through a symmetric $4f$ filtering system.

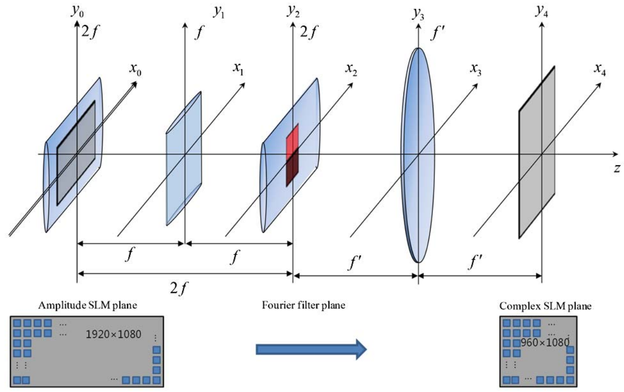

Fig. 5. Transformation of an amplitude SLM to a complex SLM through an anamorphic $4f$ filtering system.

images with the same viewing angles in the x- and y-axial directions. The oblong pixel shape would cause the viewing angle along the vertical axis to be two times wider than that along the horizontal axis. An optical transformation to create square pixels is feasible using an anamorphic system with a Fourier filter as illustrated in Fig. 5. Two cylindrical lenses with x-directional focal length $2f_1$ are laid on the amplitude SLM plane and the Fourier filter plane. A cylindrical lens with a y-directional focal length f_1 is placed in the plane intermediate between the SLM and the Fourier filter planes. The system created in this way has an anamorphic 2D Fourier transform of x-directional focal length $2f_1$ and y-directional focal length f_1 with an axial length of $2f_1$.

The 4×4 ray-transfer matrix of the anamorphic 2D Fourier transform is modeled as

$$T_{f_1} = \begin{pmatrix} 0 & 0 & 2\lambda f_1 & 0 \\ 0 & 0 & 0 & \lambda f_1 \\ \frac{1}{-2\lambda f_1} & 0 & 0 & 0 \\ 0 & \frac{1}{-\lambda f_1} & 0 & 0 \end{pmatrix}. \tag{6}$$

The total transfer matrix of the system is the product of the anamorphic Fourier transform matrix and the symmetric Fourier transform matrix of focal length f_2 given by

$$T_{f_2} \cdot T_{f_1} = \begin{pmatrix} 0 & 0 & \lambda f_2 & 0 \\ 0 & 0 & 0 & \lambda f_2 \\ \frac{1}{-\lambda f_2} & 0 & 0 & 0 \\ 0 & \frac{1}{-\lambda f_2} & 0 & 0 \end{pmatrix} \begin{pmatrix} 0 & 0 & 2\lambda f_1 & 0 \\ 0 & 0 & 0 & \lambda f_1 \\ \frac{1}{-2\lambda f_1} & 0 & 0 & 0 \\ 0 & \frac{1}{-\lambda f_1} & 0 & 0 \end{pmatrix}$$

$$= \begin{pmatrix} -f_2/(2f_1) & 0 & 0 & 0 \\ 0 & -f_2/f_1 & 0 & 0 \\ 0 & 0 & -(2f_1)/f_2 & 0 \\ 0 & 0 & 0 & -f_1/f_2 \end{pmatrix}. \tag{7}$$

The system of $T_{f_2} \cdot T_{f_1}$ is the anamorphic imaging system with x- and y-directional magnification ratios of $-f_2/(2f_1)$ and $-f_2/f_1$, respectively. The horizontal magnification is contracted to half width. The imaging characteristic is illustrated in Fig. 5. For a full-HD amplitude SLM, the resulting complex SLM has a resolution of 960×1080 and square pixels. For this system, the carrier wave in the amplitude encoding should be directed along the horizontal direction. Then, in the Fourier plane, the signal and conjugate parts are split along the horizontal direction. The SLMs with square pixels like the ones created by this scheme allow for a symmetric viewing angle in table-top holographic displays.

4. Experimental Results

The amplitude hologram encoding method is experimentally inspected by optical reconstruction of the resulting holographic images. Through the optical reconstruction of holographic images, the effective square pixel complex SLM constructed by the anamorphic transformation can be compared to the complex rectangular pixel SLM. The experimental setup is schematically depicted in Fig. 6(a). The system has two parts. The first part is the SLM module. To test the method put forward in this paper, the experiment compares complex SLMs created by the conventional system and the proposed anamorphic system. The second part is the projection imaging module, which has two parabolic mirrors resembling the $4f$ system. The diameter of each mirror is 10 in. and the focal length is 50 in. The SLM is projected on the first parabolic mirror. It is notable that at the second parabolic mirror, the modulated wave is imaged and acts as an enlarged hologram. This design has the benefit of reducing the geometric aberration even for small tilts of the optics. In this way, the performance of the holographic imaging system can be demonstrated by experiment.

The fundamental design concept of this holographic projection display system originates from the system proposed by Leister *et al.* [8]. They proposed the projection-type system to make a holographic display with a large screen size. The diffracted light from the screen converges to a point and there the viewing window is formed.

In the setup shown in Fig. 6(b), we use two large aperture concave parabolic mirrors to separate the functions. One is imaging the hologram from the SLM plane and the other collects the diffracted wave to a point on the viewing window plane. This modification has the benefit of decreasing the aberration caused by the parabolic mirrors. The second reflection makes the wave converge to the viewing window. An Epson L3C07U-8x LCD module that has 1920×1080 pixels with a pixel pitch of 8.5 μm is used as a light modulation device. A He–Ne laser with a wavelength of 543 nm is used as a coherent light source. The laser light generated from the source is collimated by pinhole collimation. Next, the collimated light passes through the SLM and Fourier lenses in turn. It is then reflected from the first parabolic mirror into a second parabolic mirror of almost identical width. After being reflected by the second mirror, the object wave converges toward the focal region where there is a narrow viewing window.

In the first experiment, we inspected the validity of the CGH encoding scheme. The experimental observation of a CGH 3D image [16,17] through a symmetric $4f$ filter is presented as shown in Fig. 7. The target image with depth information denoted in yellow and hologram pattern on the amplitude SLM are shown in Figs. 7(a) and 7(b), respectively. At each corner, small flower-shaped patterns are placed and the

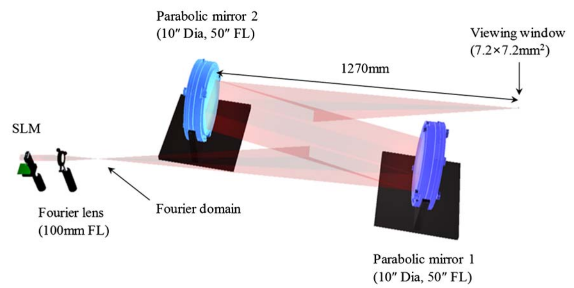

(a)

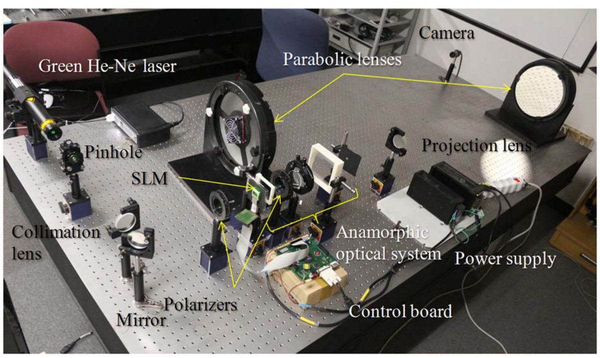

(b)

Fig. 6. Holographic imaging system: (a) schematic description and (b) experimental setup.

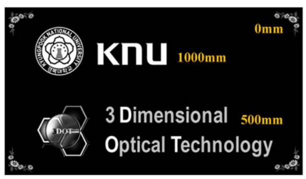

(a)

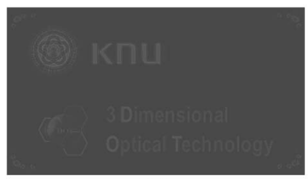

(b)

(c)

Fig. 7. Optical reconstruction experiment in the holographic imaging system with a symmetric $4f$ filter: (a) target image (1920×1080 size with a pixel pitch of 8.5 μm), (b) CGH pattern, and (c) captured images with focuses at different distances of 0, 500, and 1000 mm from the second mirror.

corresponding layer is located on the second mirror. The emblems including “KNU” and “3 Dimensional Optical Technology” are positioned at 1000 and 500 mm in front of the mirror, respectively, because the depth-discrimination effect is the main concern of this experiment. The accommodation effect was demonstrated at three different focuses including 0, 500, and 1000 mm. The labels on the right side of each figure indicate the physical distances. The captured images show the depth-discrimination effect clearly. Therefore, these results are consistent with our predictions, and consequently, the encoding method described in Section 2 is verified.

In the second experiment, the anamorphic transformation system generating an effective square pixel SLM was implemented and compared with the symmetric 4f system. In this case, for experimental convenience, we prepared a slightly modified version of, but equivalent optical setup to, the setup shown in Fig. 5. Figures 8(a) and 8(b) show a photograph and schematic of the alternative experimental setup, which is composed of three cylindrical lenses with focal lengths of $f_1 = 500$ mm, $f_3 = 150$ mm, and $f_4 = 130$ mm, and a spherical lens with a focal length of $f_2 = 500$ mm; the distances between the optical elements are set to $d_1 = 33.2$ mm, $d_2 = 104.5$ mm, $d_3 = 112.7$ mm, and $d_4 = 108.1$ mm, respectively. Hence, the effective focal length in the x axis becomes two times bigger than that in the y axis. The fourth lens at the focal plane is chosen to make the diverging phases in the x axis and y axis equal to each other. So the optical function of the system coincides with the one shown in Fig. 5.

By use of the anamorphic optical transformation, the shape of the pixel is defined as a square. Through comparisons, there is an advantage of the rectangular shaped pixel. The shape of the viewing window also becomes a square because the viewing window is located at the focal point. The square shape is more appropriate for covering the iris of the eye.

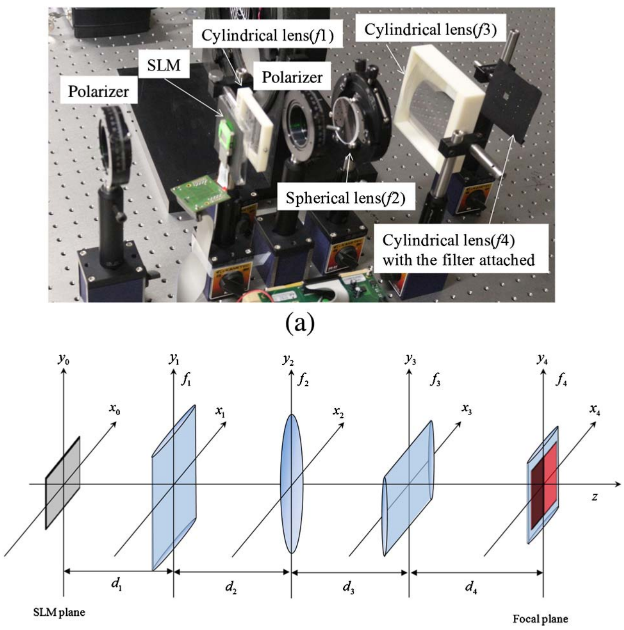

(b)

Fig. 8. Implementation of the anamorphic optical transformation model: (a) experimental implementation and (b) schematic of the optical system.

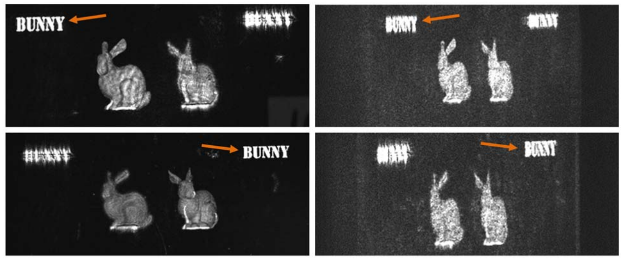

(a) (b)

Fig. 9. Comparison of the (a) numerical reconstruction and (b) optical reconstruction.

Amplitude CGHs were generated that contained two 3D bunny models accompanied by letters and separated from each other by depth. Figure 9 shows a comparison of the optical reconstructions of the symmetric 4f system and those of the anamorphic system. In both upper figures, the left object and letters are in focus and the right object and letters are out of focus. Conversely, in both lower figures, the right object and letters are in focus. In the optical reconstruction, there is intrinsic speckle noise but nevertheless the result shown in Fig. 9(b) demonstrates that the anamorphic optical transformation of the wide-screen amplitude SLM to a square pixel complex SLM has been successful. It was confirmed that the pixel shape is square. The horizontal magnification ratio is half of the vertical one. The holographic imaging effects are well preserved. In practice, the number of the optical components used to construct the anamorphic system is more than that of the symmetric optical system. Thus, the additional aberration, surface scattering, and undesired reflections degrade the image quality.

5. Conclusion

In conclusion, we have analyzed various theoretical aspects of amplitude CGH encoding associated with the amplitude macro-pixel structure and proposed a design for an optical system that transforms an amplitude SLM to an effective complex SLM with square pixels. It was experimentally demonstrated that the amplitude CGH encoding scheme produces low noise holographic 3D images with a clear depth-discrimination effect and that the formation of a square pixel complex SLM can be achieved through an anamorphic optical filter, which can generate full-parallax holographic images with symmetric vertical–horizontal viewing angles.

This work was supported by the GigaKOREA project (GK13D0100, Development of Telecommunications Terminal with Digital Holographic Table-Top Display).

References

1. J. Hong, Y. Kim, H.-J. Choi, J. Hahn, J.-H. Park, H. Kim, S.-W. Min, N. Chen, and B. Lee, "Three-dimensional display technologies of recent interest: principles, status, and issues," Appl. Opt. **50**, H87–H115 (2011).
2. P. St.-Hilaire, S. A. Benton, M. Lucente, and P. M. Hubel, "Color images with the MIT holographic video display," Proc. SPIE **1667**, 73–84 (1992).
3. K. Maeno, N. Fukaya, O. Nishikawa, K. Sato, and T. Honda, "Electro-holographic display using 15 mega pixels LCD," Proc. SPIE **2652**, 15–23 (1996).
4. M. Stanley, R. W. Bannister, C. D. Cameron, S. D. Coomber, I. G. Cresswell, J. R. Hughes, V. Hui, P. O. Jackson, K. A. Milham, R. J. Miller, D. A. Payne, J. Quarrel, D. C. Scattergood, A. P. Smith, M. A. Smith, D. L. Tipton, P. J. Watson, P. J. Webber, and C. W. Slinger, "100 mega-pixel computer generated holographic images from active tiling: a dynamic and scalable electro-optic modulator system," Proc. SPIE **5005**, 247–258 (2003).
5. J. Hahn, H. Kim, Y. Lim, G. Park, and B. Lee, "Wide viewing angle dynamic holographic stereogram with a curved array of spatial light modulators," Opt. Express **16**, 12372–12386 (2008).
6. G. Finke, T. Kozacki, and M. Kujawinska, "Wide viewing angle holographic display with multi spatial light modulator array," Proc. SPIE **7723**, 77230A (2010).
7. F. Yaraş, H. Kang, and L. Onural, "Circular holographic video display system," Opt. Express **19**, 9147–9156 (2011).
8. N. Leister, A. Schwerdtner, G. Füutterer, S. Buschbeck, J.-C. Olaya, and S. Flon, "Full-color interactive holographic projection system for large 3D scene reconstruction," Proc. SPIE **6911**, 69110V (2008).
9. B. R. Brown and A. W. Lohmann, "Complex spatial filtering with binary masks," Appl. Opt. **5**, 967–969 (1966).
10. C. B. Burckhardt, "A simplification of Lee's method of generating holograms by computer," Appl. Opt. **9**, 1949 (1970).
11. V. Arrizón, G. Méndez, and D. Sánchez-de-La-Llave, "Accurate encoding of arbitrary complex fields with amplitude-only liquid crystal spatial light modulators," Opt. Express **13**, 7913–7927 (2005).
12. C. K. Hsueh and A. A. Sawchuck, "Computer-generated double phase holograms," Appl. Opt. **17**, 3874–3883 (1978).
13. H. Song, G. Sung, S. Choi, K. Won, H.-S. Lee, and H. Kim, "Optimal synthesis of double phase computer generated holograms using a phase-only spatial light modulator with grating filter," Opt. Express **20**, 29844–29853 (2012).
14. O. Bryngdahl and A. Lohmann, "Single-sideband holography," J. Opt. Soc. Am. **58**, 620–624 (1968).
15. J. Goodman, *Introduction to Fourier Optics*, 2nd ed. (McGraw-Hill, 1996).
16. H. Kim, J. Hahn, and B. Lee, "Mathematical modeling of triangle-mesh-modeled three-dimensional surface objects for digital holography," Appl. Opt. **47**, D117–D127 (2008).
17. D. Im, E. Moon, Y. Park, D. Lee, J. Hahn, and H. Kim, "Phase regularized polygon computer-generated holograms," Opt. Lett. **39**, 3642–3645 (2014).